miR-149 Suppresses Breast Cancer Metastasis by Blocking Paracrine Interactions with Macrophages

Ismael Sánchez-González[1], Anja Bobien[1], Christian Molnar[1], Simone Schmid[1], Michaela Strotbek[1], Melanie Boerries[2,3,4,5], Hauke Busch[6], and Monilola A. Olayioye[1,7]

ABSTRACT

Paracrine activation of cells contained in the tumor microenvironment promotes tumor progression and metastasis. In breast cancer, malignant cells recruit and educate macrophages into a M2 tumor–promoting phenotype that supports the metastatic spread of cancer cells. Here, we show that miR-149 functions as a metastasis-suppressing microRNA in breast cancer cells by limiting colony-stimulating factor-1 (CSF1)–dependent recruitment and M2 polarization of macrophages. In lymph node–positive, triple-negative breast cancer (TNBC) tissues, low miR-149 expression correlated with macrophage infiltration and reduced patient survival. By directly targeting CSF1, miR-149 expression in TNBC cell lines (MDA-MB-231 and BT-549) inhibited the recruitment of human monocytic THP-1 cells and primary human macrophages. Furthermore, in macrophages cocultured with MDA-MB-231 cells expressing miR-149, epidermal growth factor (EGF) and amphiregulin expression levels were strongly reduced, resulting in reduced EGF receptor activation in the cancer cells. *In vivo*, lung metastases developing from orthotopic MDA-MB-231 tumors were reduced by 75% by miR-149 expression, and this was associated with impaired M2 macrophage infiltration of the primary tumors. These data suggest that miR-149 downregulation functionally contributes to breast tumor progression by recruiting macrophages to the tumor and facilitating CSF1 and EGF receptor cross-talk between cancer cells and macrophages.

Significance: These findings contribute to the understanding of tumor–stroma interactions by showing that miR-149 downregulation in TNBC enhances reciprocal growth factor signaling between macrophages and cancer cells, which promotes tumor progression and metastasis.

Graphical Abstract: http://cancerres.aacrjournals.org/content/canres/80/6/1330/F1.large.jpg.

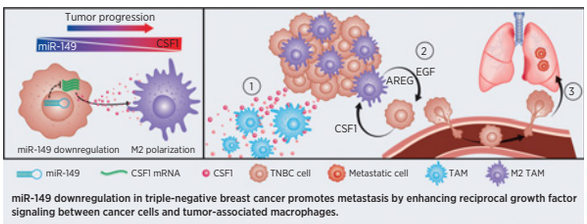

miR-149 downregulation in triple-negative breast cancer promotes metastasis by enhancing reciprocal growth factor signaling between cancer cells and tumor-associated macrophages.

Introduction

Metastasis is a complex multistep process during tumor progression and represents the main cause of death in cancer patients (1). Triple-negative breast cancer (TNBC), constituting 20% of all breast cancer cases, is defined by the lack of hormone receptor expression and ErbB2/HER2 amplification/overexpression. Compared with other breast cancer subtypes, TNBC is associated with higher recurrence and metastatic potential (2, 3). Over the last years, the intricate balance of interactions between cancer cells and the tumor microenvironment has emerged as a crucial regulator of tumor progression and metastasis (4, 5). Tumor-associated macrophages (TAM) are major constituents of the tumor–stroma in various solid tumors, including prostate, bladder, colon, and breast cancers (6, 7). In response to microenvironmental stimuli, TAMs polarize toward classically (M1) or alternatively (M2) activated cells, with tumoricidal or tumor-promoting properties, respectively (5).

TAMs are recruited to tumors in response to diverse tumor-derived chemotactic factors. Colony-stimulating factor-1 (CSF1) in particular is abundantly expressed in TNBC and, via its receptor CSF1R, regulates macrophage survival, migration, and differentiation, and induces a tumor-promoting M2 phenotype (8). Furthermore, CSF1R stimulation of TAMs induces the secretion of factors such as epidermal growth factor (EGF), thereby engaging TAMs in a paracrine signaling loop with breast cancer cells. EGF in turn promotes cancer cell proliferation and the formation of invadopodia, eventually leading to intravasation of breast cancer cells (9). Intravital multiphoton imaging of xenograft mouse models has shown that macrophages are required for primary breast tumor invasion (10), and in the absence of CSF1, tumor progression and metastasis are reduced (11, 12). In breast cancer patients, CSF1R overexpression and infiltrating M2 TAMs correlate with poor outcome (13–15). Although paracrine CSF1 and EGF receptor interactions critically contribute to breast tumor

[1]Institute of Cell Biology and Immunology, University of Stuttgart, Stuttgart, Germany. [2]Institute of Medical Bioinformatics and Systems Medicine, Medical Center, University of Freiburg, Faculty of Medicine, University of Freiburg, Freiburg, Germany. [3]German Cancer Consortium (DKTK) and German Cancer Research Center (DKFZ), Heidelberg, Germany. [4]Institute of Molecular Medicine and Cell Research, Albert-Ludwigs-University Freiburg, Freiburg, Germany. [5]Comprehensive Cancer Center Freiburg (CCCF), Medical Center, University of Freiburg, Faculty of Medicine, University of Freiburg, Freiburg, Germany. [6]Lübeck Institute of Experimental Dermatology and Institute of Cardiogenetics, University of Lübeck, Lübeck, Germany. [7]Stuttgart Research Center Systems Biology (SRCSB), University of Stuttgart, Stuttgart, Germany.

Note: Supplementary data for this article are available at Cancer Research Online (http://cancerres.aacrjournals.org/).

Corresponding Author: Monilola A. Olayioye, University of Stuttgart, Allmandring 31, Stuttgart 70569, Germany. Phone: 49-711-685-69301; Fax: 49-711-685-67484; E-mail: monilola.olayioye@izi.uni-stuttgart.de

Cancer Res 2020;80:1330–41

doi: 10.1158/0008-5472.CAN-19-1934

progression, the molecular mechanisms involved in establishing and maintaining these signaling loops are still poorly understood.

MicroRNAs (miRNA) are small noncoding RNAs of 17–24 nucleotides in length that regulate gene expression at the posttranscriptional level (16, 17). MiRNAs act by binding to their target mRNAs usually within the 3′-untranslated region (3′-UTR), resulting in translational repression and/or mRNA degradation (16). MiRNA dysregulation plays a key role in tumorigenesis and tumor progression. Although certain upregulated miRNAs have been characterized to possess transforming potential, there are other miRNAs with inherent tumor-suppressive activity that are downregulated in cancer cells (18, 19). In different cancer types, miR-149 expression has been reported to be altered. For example, in nasopharyngeal cancer and melanoma miR-149 is upregulated, whereas in most solid cancers, including breast cancer, miR-149 is found to be downregulated (20). We as well as others have reported that in TNBC miR-149 expression levels inversely correlate with higher tumor stage and that miR-149 regulates signaling molecules downstream of integrin receptors, as shown by experiments performed with the TNBC cell line MDA-MB-231 (21, 22). In this study, we identify CSF1 as a novel miR-149 target and demonstrate that miR-149 reexpression in MDA-MB-231 cells impairs paracrine interactions of the tumor cells with primary macrophages both *in vitro* and *in vivo*.

Materials and Methods

Cell culture and transfection

The cell lines MDA-MB-231 and BT-549 were obtained from CLS, Hs578T from Dr. Bernhard Lüscher (RWTH Aachen), and THP-1 from DSMZ. All cell lines were tested negative for *Mycoplasma* (Lonza, LT07-318) and authenticated (Multiplexion GmbH). Cell lines were cultured in RPMI-1640 (Life Technologies) supplemented with 10% FCS (PAA Laboratories) at 37°C, 5% CO_2, and 90% humidity. THP-1 cells were differentiated by treatment with 25 nmol/L phorbol 12,13-dibutyrate (PDBu) for 48 hours, followed by a 24-hour rest period in fresh media. Transient transfections of miRNA mimics or siRNAs were performed at final concentrations of 5 nmol/L and 10 nmol/L, respectively, using RNAiMax (Life Technologies). The miR-149 mimic RNA is a double-stranded oligonucleotide corresponding to the mature miRNA sequence of hsa-miR-149-5p (cat. #c-300631-07, UCUGGCUCCGUGUCUUCACUCCC). miR-149 and miRNA-negative control#1 (miR-con, cat. #CN-001000-01) were obtained from Dharmacon. Silencer Select siRNAs targeting CSF1 (cat. # 4392420) and the negative control (cat. #4390843) were obtained from Life Technologies. Plasmid transfection was performed using Lipofectamine LTX with Plus Reagent (Life Technologies). For stable cell lines, MDA-MB-231 cells were transfected with pcDNA6.2-GW/EmGFP-miRNA vectors and selected with 1 μg/mL Blasticidin S (Life Technologies) for 2 weeks. GFP-positive cells were enriched by fluorescence activated sorting (BD Bioscience, FACSAria III), and miR-149 overexpression was then confirmed by qPCR. Conditioned medium (CM) was obtained by exchanging the medium on MDA-MB-231 cells (80% confluency) with 3 mL of fresh growth medium containing 10% FCS. After 24 hours, the cell culture supernatant was collected, centrifuged, and used immediately. Doubly conditioned medium (DCM) was obtained by first incubating 1×10^6 THP-1 MΦs with CM (2.5 mL) derived from MDA-MB-231 cells for 24 hours, followed by medium exchange (RPMI plus 10% FCS, 2.5 mL) and collection of the cell culture supernatant after 24 hours. At the time of CM/DCM collection, the cells were counted to ensure conditioning of the medium by comparable cell numbers.

Monocyte isolation and macrophage differentiation

Buffy coats were obtained from healthy donors (provided by the Katherinenhospital, Stuttgart, Germany), and peripheral blood mononuclear cells (PBMC) were isolated by centrifugation in Ficoll (PromoCell), followed by positive selection with anti-CD14 magnetic beads (Miltenyi Biotec) according to the manufacturer's instructions. For human primary macrophage differentiation (hMΦ), CD14-positive monocytes were cultured in RPMI containing 20% human serum (Zentrum für Klinische Transfusionsmedizin, Tübingen, Germany) at 37°C, 5% CO_2, and 90% humidity for at least 7 days with medium exchange every 3 to 4 days as previously described (23).

Transwell cocultures

For cocultures with primary human macrophages, 1×10^6 MDA-MB-231 cells were seeded in 1 mL RPMI containing 10% human serum into the upper Transwell chamber (0.4-μm pore size; Greiner Bio-One) and allowed to adhere overnight. The next day, 1×10^6 hMΦ in 1-mL RPMI containing 10% human serum were seeded into the lower well and the coculture was incubated for 24 hours. Transwell cocultures of THP-1 and MDA-MB-231 cells were performed as described by Stewart and colleagues (24).

Three-dimensional tumor spheroid coculture assays

MDA-MB-231 cells were labeled with CellTracker Green (Invitrogen) and seeded in GravityTRAP ULA plates (InSphero) in RPMI containing 10% FCS and 2.5% Matrigel. After 72 hours, single spheroids were harvested and seeded in RPMI containing 2.5% Matrigel on top of collagen R bed (1 mg/mL, Serva) containing 1.6×10^4 THP-1 MΦ labeled with CellTracker Orange (Invitrogen). Z-stack images of the spheroids (at 5-μm intervals and optical slices starting at the bottom of the spheroid) were acquired on a Zeiss Cell Observer Spinning Disk microscope equipped with a Plan-Apochromat 10×/0.45 and an Axiocam 503 monocamera. 3D-spheroid reconstruction was done with Zen blue 2.3 software.

Migration, invasion, and proliferation assays

For migration, 5×10^4 cells were seeded in medium containing 0.5% FCS into Transwells (8-μm pore size, Costar) and allowed to migrate for 3 hours (THP-1 MΦ) or 4 hours (MDA-MB-231). For invasion, Transwells were coated on the upper side with 50 μL growth factor–reduced Matrigel (BD Biosciences) diluted 1:20 in medium containing 0.5% FCS, followed by seeding of MDA-MB-231 cells (5×10^4) in medium containing 0.5% FCS and overnight incubation. Cells on the underside of the membranes were fixed, stained with crystal violet, and six independent fields at a ×10 magnification were quantified. For proliferation, 1×10^3 cells were plated into 96-well plates, and cell proliferation was assessed every 24 hours for 4 days by CellTiter-Glo Luminescent Cell Viability Assay (Promega).

ELISA assays

The concentration of CSF1 in the CM of TNBC cell lines was measured with the human CSF1 ELISA Kit #EHCSF1 (Thermo Scientific) according to the manufacturer's instructions.

Luciferase reporter assay

HEK293T cells (3×10^4) per well were seeded into 96-well plates. The next day, cells were transfected with 10 ng pGL3-firefly luciferase plasmids (wt/mut) together with 10 ng pRL-*Renilla* luciferase plasmid and 50 nmol/L miR-con or miR-149 mimics using Lipofectamine 2000 (Invitrogen). Two days later, cells were lysed with passive lysis buffer (Promega). The activities of the luciferases were measured by

sequential substrate addition as described by Dyer and colleagues (25) and detection at 562 nm with the multimode reader Infinite 200 PRO (Tecan). Firefly luciferase activities were normalized to those of *Renilla* luciferase activities in each sample. Experiments were done with at least triplicate samples.

Animal experiments

MDA-MB-231 cells (2×10^6) were implanted into the fourth mammary fat pad of 8-week-old female SCID mice (Janvier Labs). Tumor growth was determined three times per week with a digital Vernier caliper, and tumor volume was calculated as follows: tumor volume $= 0.5 \times (\text{length} \times (\text{width})^2)$. Mice were sacrificed after 6 1/2 weeks. Animal care and experiments were conducted based on protocols approved by Institutional Animal Care and Use Committee and state authorities.

Tissue immunostaining

Primary tumors and lungs were isolated, snap-frozen in optimal cutting temperature medium (Sakura Finetek), and 8-μm (tumors) or 12-μm (lungs) sections were prepared. Blocking was performed with 5% goat serum for 1 hour. Tissues were incubated at 4°C overnight with primary antibodies, followed by three washing steps with 1× TBS (0.05 mol/L Trizma base and 0.15 mol/L sodium chloride, pH 7.6). Tissues were incubated with Alexa Fluor 546 or 633 conjugated secondary antibodies for 1 hour at room temperature, nuclei were counterstained with DAPI and samples were mounted in Fluoromount G (Southern Biotech). Imaging was performed on a Zeiss Cell Observer Spinning Disk microscope equipped with a Plan-Apochromat 20×/0.8 for tumor or with a Plan-Apochromat 10×/0.45 for lung sections and an Axiocam 503 monocamera. F4/80-, CD206-, and vimentin-positive areas were quantified by ImageJ (v1.49s).

miRNA-target prediction, Kaplan–Meier plot, and correlation analyses

Gene expression from breast cancer tumors and matched normal probes were obtained from The Cancer Genome Atlas (TCGA) as raw counts (26). Libraries were normalized, and count values were converted to counts per million (cpm) values using edgeR. TNBC samples were selected according to the combined negative status of the variables PR_Status/HER2_Final_Status/ER_Status. Lymph node-positive samples were distinguished according to the pathologic_N variable as follows: N0 = no cancer or cancer areas < 0.2 mm, N1 = 1–3, N2 = 4–9, N3 = >10 affected axillary lymph nodes. We excluded cases where lymph nodes were not evaluated. Survival data of the BRCA patients were obtained from Oncolnc (27). Kaplan–Meier curves and survival significance was calculated using the R library survival in version 2.44. Target genes of miR-149 were predicted through the miRWalk2.0 database (28). Genes were selected as miR-149 targets, if such an interaction was predicted in the 3′-UTR region by at least 6 of 12 databases with a P value of <0.05. Functional enrichment for biological processes (BP) within the Gene Ontology (GO; refs. 29, 30) was calculated via a conditional hypergeometric test of the target genes as implemented in the R GOstats library.

Statistical analysis

Unless stated otherwise, all data represent the mean of three experiments ± SD. Statistical significance was analyzed by t test and one-way ANOVA followed by Tukey posttest (GraphPad Prism version 4.03). P values below 0.05 were considered significant (*, $P < 0.05$; **, $P < 0.01$; ***, $P < 0.001$), $P > 0.05$; ns, not significant.

See Supplementary Information for vectors and cloning, RNA and protein analyses, oligos and antibodies (Supplementary Tables S1 and S2) and supplementary figure legends.

Results

miR-149 and survival of TNBC patients

We analyzed the overall survival of 987 breast cancer patients from TCGA with respect to lymph node metastasis, TNBC status, and expression strength of miR-149 [**Fig. 1A**; TNBC-negative (top), TNBC-positive (bottom)]. An additive Cox proportional hazards regression model on these variables clearly indicates significantly poorer survival in the presence of lymph node metastasis (HR = 2.30, $P = 1.1 \times 10^{-6}$), TNBC-positive cancer (HR = 1.81, $P = 0.027$) and low expression of miR-149 (HR = 1.59, $P = 0.013$). To further elucidate the functional role of miR-149 in breast cancer, we predicted putative target genes of miR-149 through miRWalk2.0 (28), a database for predicted and validated miRNA-target interactions. Genes were selected as target genes, if an interaction was predicted in the 3′-UTR region by at least 6 of 12 databases with a P value of <0.05. This resulted in 2,644 unique target genes. It has been suggested that miRNAs preferentially target groups of functionally related mRNAs (31). In the following, we used this idea to narrow down the number of putative miR-149 targets in a two-step process. First, we tested for significantly enriched GO terms using a conditional hypergeometric test. This revealed an enrichment of 474 GO terms ($P < 0.05$), which were mainly related to cell morphogenesis, development, differentiation, cell–cell adhesion, migration, and immune system development. Next, we searched for overrepresented genes within the enriched GO terms. Out of the 2,644 predicted targets, 30% did not belong to any GO term, but 5% (96 genes) of the predicted targets belonged to 45 or more terms. We hypothesized that the latter target genes are biologically most meaningful due to the simultaneous regulation of genes in the same pathway through miR-149. Importantly, the expression of only five of these genes (CSF1, VAV1, SEMA4D, EGFR, and PRTPO) was significantly anticorrelated with that of miR-149 in the lymph node-positive TNBC tissue samples (Supplementary Fig. S1A). Transfection of the TNBC cell line MDA-MB-231 with miR-149 mimics followed by RT-qPCR analysis of these five genes revealed suppression of semaphorin 4D (SEMA4D) and CSF1 transcript levels by miR-149, whereas no regulation was observed for the guanine nucleotide exchange factor VAV1 and EGFR, and protein tyrosine phosphatase receptor–type O (PTPRO) was not expressed (**Fig. 1B**). CSF1 and SEMA4D play important roles in tumor–stroma interactions, with CSF1 stimulating macrophage survival, recruitment, and differentiation (8) and SEMA4D stimulating angiogenesis by binding to plexin-B1 receptors on endothelial cells (32). To explore *in silico* the possibility of miR-149 expression regulating cancer cell interactions with macrophages or endothelial cells, we performed a cell-enrichment analysis based on the bulk gene expression of the tumor samples (33). Intriguingly, among the immune cells, monocytes and macrophages were strongly and significantly anticorrelated with miR-149 expression, whereas endothelial cell abundance was less prominently and significantly regulated with respect to miR-149 expression (**Fig. 1C**). Considering the association of low miR-149 levels with higher macrophage presence particularly in lymph node–positive patients (**Fig. 1D**) and the presence of three conserved miR-149 binding sites within the 3′-UTR of CSF1 (Supplementary Fig. S1B), we decided to focus on the regulation of TNBC-macrophage interactions by miR-149.

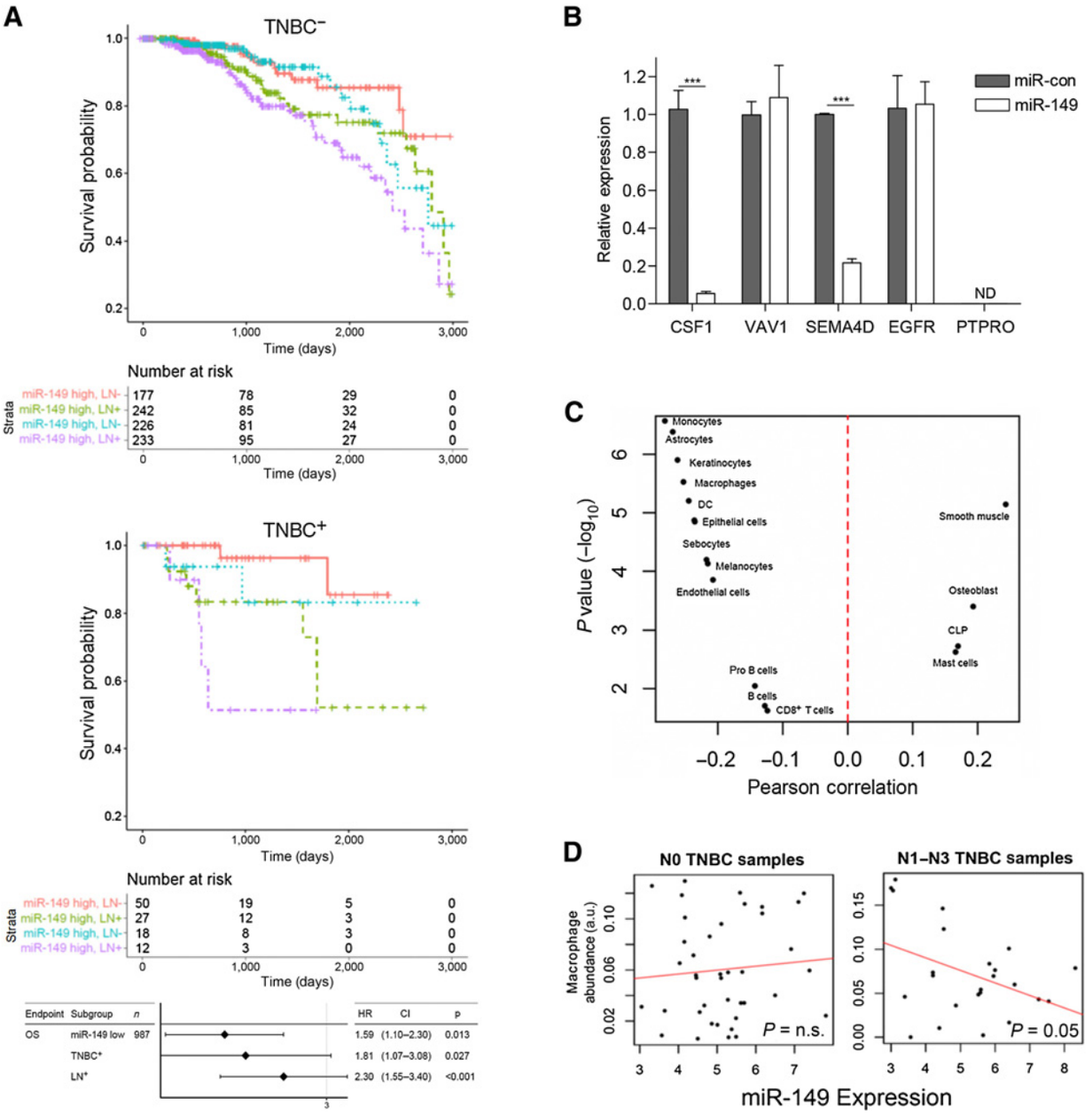

Figure 1.

Low miR-149 expression in lymph node–positive TNBC tissues correlates with poor prognosis and macrophage infiltration. **A,** Kaplan–Meier curves for the survival of breast cancer patients from the TCGA database. Top, $TNBC^-$ patients; bottom, $TNBC^+$ patients. Forest tree plot of hazard ratio (HR) with 95% confidence interval (CI) and *P* values denote the significance for different survival of the individual variables based on a Cox proportional hazards regression model. Strata were high/low miR-149 expression, lymph node metastasis (LN +/−), and classification into TNBC +/− based on the reported expression of progesterone/estrogen receptor and HER2 status. **B,** MDA-MB-231 cells were transiently transfected with miR-con or miR-149 mimics. Three days after transfection, RNA was extracted, and the relative transcript levels of the indicated genes were determined by qRT-PCR. Peptidylprolyl isomerase A and ACTB were used as reference genes. Data, mean ± SD, $n = 3$. ***, $P \leq 0.001$; unpaired two-tailed Student *t* test. **C,** The scatter plot depicts the Pearson correlation coefficient between miR-149 abundance and cell-enrichment scores versus the associated cell-enrichment *P* value significance. **D,** Correlation of the predicted macrophage abundance and miR-149 expression in lymph node-negative (N0) and lymph node-positive tumor samples (N1–N3). The line indicates a linear regression to the data points of the tumor samples. n.s., nonsignificant.

miR-149 overexpression in MDA-MB-231 spheroids impairs THP-1 macrophage recruitment

To investigate if miR-149 expression in breast cancer cells regulates the interaction with macrophages, we established a 3D coculture migration assay in which breast cancer cell spheroids in Matrigel-containing serum-free medium were placed on top of a collagen bed containing THP-1 macrophages (**Fig. 2A**). MDA-MB-231 cells produce CSF1 and are known to readily attract macrophages (12).

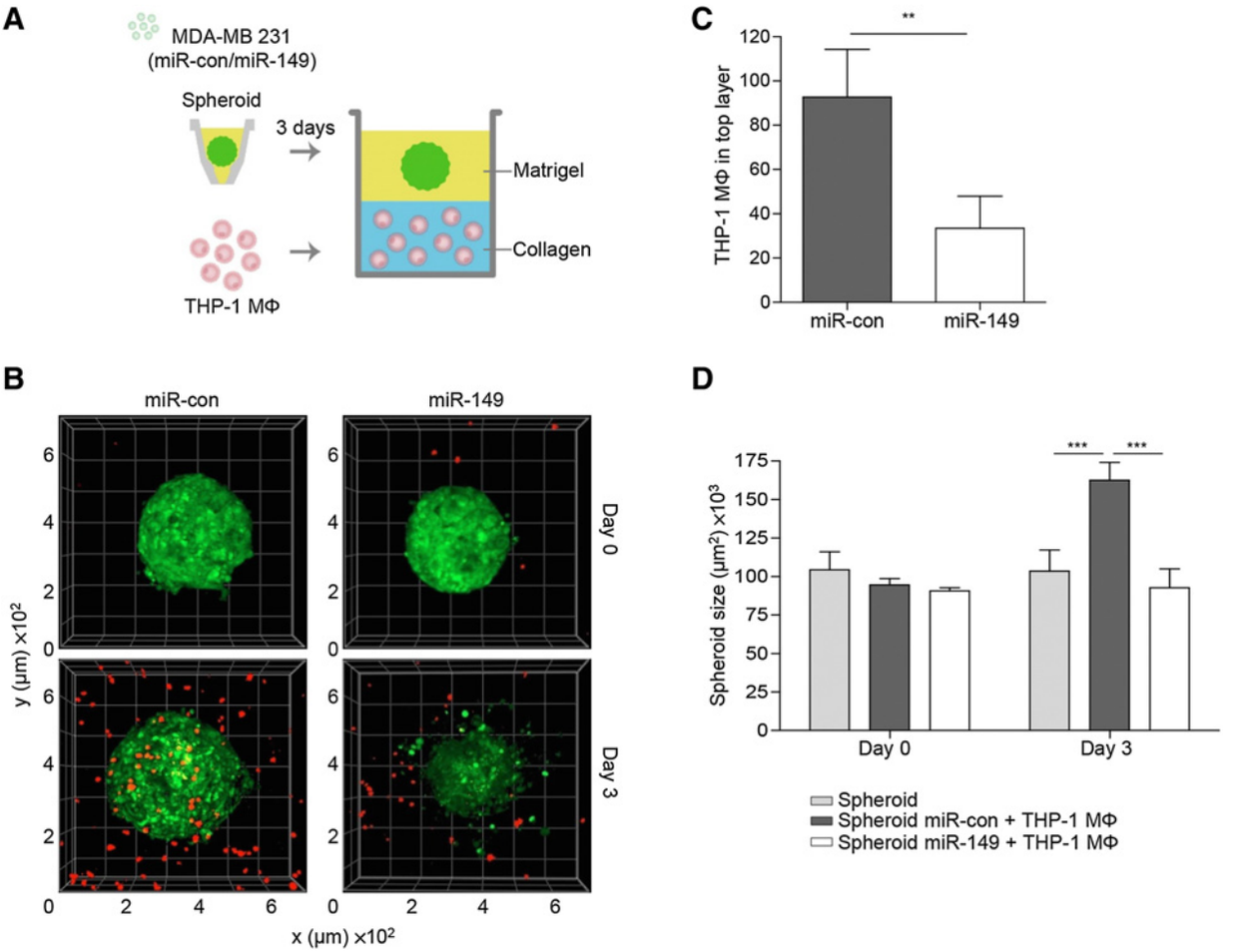

Figure 2.

miR-149 reduces THP-1 macrophage recruitment to MDA-MB-231 spheroids. **A,** Scheme of the workflow. MDA-MB-231 cells were transiently transfected with miR-con or miR-149 mimics, labeled with CellTracker Green, and seeded in a GravityTRAP plate for spheroid formation. After 3 days, spheroids were harvested and seeded in Matrigel-containing medium on top of a collagen bed containing THP-1 cells differentiated by phorbol ester (PDBu) treatment (THP-1 MΦ) and labeled with CellTracker Orange. **B,** At days 0 and 3 of the coculture, the spheroid contained in the top layer was imaged with a spinning disk confocal microscope (30 Z-stacks, 5-μm intervals) and Z-stacks were used for 3D reconstruction using the ZEN software. **C** and **D,** The total number of THP-1 MΦ in the individual Z-stacks of the top layer was quantified (**C**) and the spheroid size (**D**) was determined by analysis of the cross-section area of the most distal Z-stack using the ZEN software. Data, mean ± SD; 12 spheroids per condition from three independent experiments. **, $P \leq 0.01$; ***, $P \leq 0.001$; unpaired two-tailed Student *t* test (**C**) and one-way ANOVA (**D**).

Spheroids were generated by culturing MDA-MB-231 cells transfected with control miRNA (miR-con) or miR-149 and labeled with a green CellTracker dye in GravityTrap plates for 48 hours. As a model for macrophages, we used THP-1 cells, a monocytic leukemia cell line that differentiates into CD11b-positive macrophages (THP-1 MΦ) in response to phorbol ester (PDBu) treatment (34, 35). After 3 days of coculture, THP-1 MΦ (labeled in red) had efficiently migrated into the top spheroid-containing layer, with a subset of THP-1 MΦ also found to infiltrate the control spheroids (**Fig. 2A**; Supplementary Fig. S2A, left). Compared with the control, the number of THP-1 MΦ attracted by MDA-MB-231 spheroids transfected with miR-149 mimics was significantly reduced (**Fig. 2B** and **C**). We further observed that the coculture with THP-1 MΦ stimulated the growth of MDA-MB-231 spheroids expressing miR-con when compared with that of spheroids in monoculture, whereas no increase in size was observed in cocultured MDA-MB-231 spheroids expressing miR-149 (**Fig. 2D**). Of note, neither miR-con nor miR-149 mimics affected proliferation, as spheroids at day 0 were comparable in size to their nontransfected counterparts (**Fig. 2D**, left). This is in line with our previous observations on proliferation rates of MDA-MB-231 cells not being affected by miR-149 (21). Taken together, these findings suggest that the presence of miR-149 in breast cancer cells inhibits macrophage recruitment and macrophage-induced tumor cell proliferation.

CSF1 is a direct target of miR-149

To validate CSF1 as a miR-149 target we performed luciferase reporter gene assays. To this end, wild-type (WT) and mutated (mut) 3′-UTR sequences of the CSF1 gene were cloned downstream of the luciferase gene in the pGL3 reporter vector. HEK293T cells were transfected with these constructs along with miR-con or miR-149, and luciferase activity was measured 3 days later. Whereas luciferase activity was strongly reduced by miR-149 mimics in the case of the WT construct, upon deletion of the three predicted miR-149 binding sites (mut), miR-149 was no longer able to suppress luciferase activity

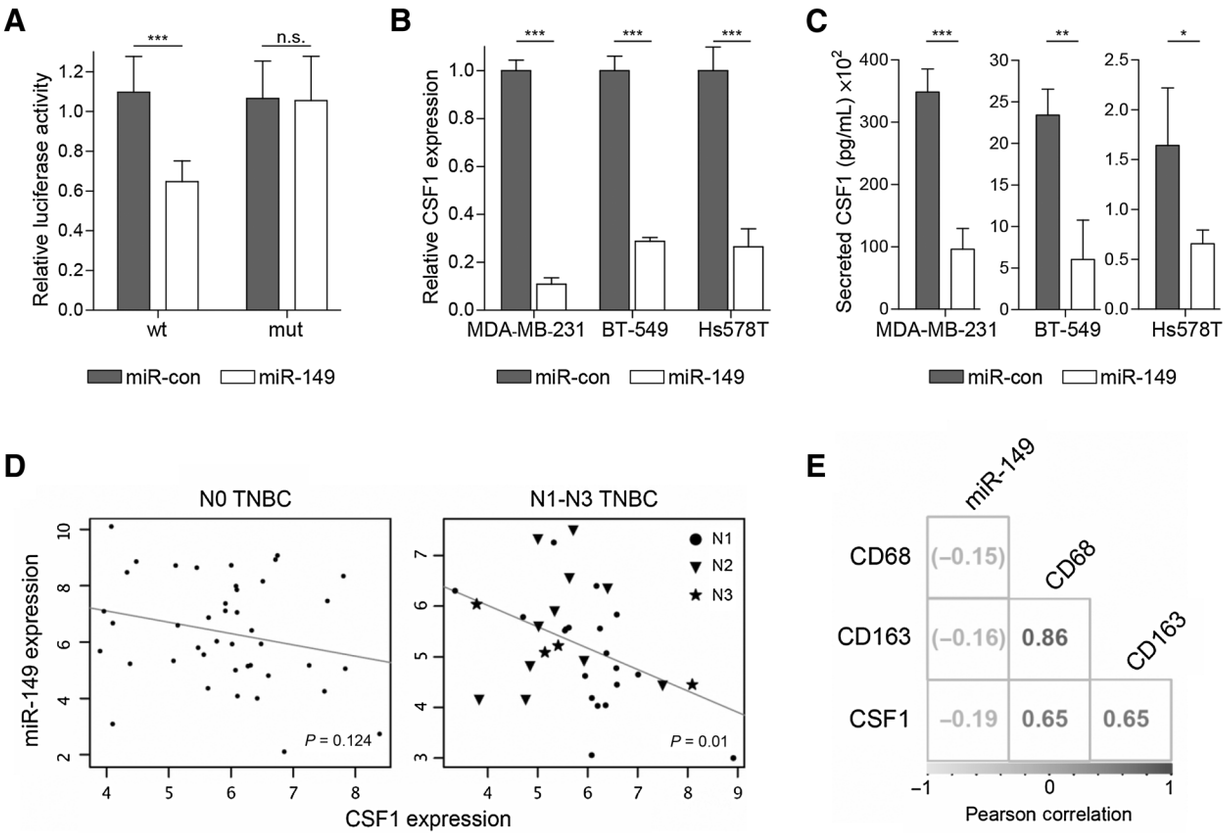

Figure 3.

miR-149 directly targets CSF1 and inversely correlates with CSF1 expression in TNBC tissues. **A,** HEK293T cells were cotransfected with wild-type (WT) or mutant (mut) CSF1 3′-UTR reporter constructs along with miR-con or miR-149 mimics. Three days after transfection, cells were lysed and luciferase activity was measured. **B** and **C,** TNBC cell lines were transiently transfected with miR-con or miR-149 mimics. Three days after transfection, CSF1 transcript levels were determined by qRT-PCR (peptidylprolyl isomerase A and beta actin were used as reference genes; **B**) or CM was generated (**C**), and levels of secreted CSF1 protein were quantified by ELISA. Data, mean ± SD, $n = 3$. *, $P \leq 0.05$; **, $P \leq 0.01$; ***, $P \leq 0.001$; unpaired two-tailored Student t test. **D,** Inverse correlation of miR-149 and CSF1 transcript levels in lymph node–negative (N0) and lymph node–positive (N1–N3) human TNBC tissues. **E,** Pearson correlation between mir-149, CSF1, and the macrophage markers CD68 and CD163 in TNBC samples. Brackets, not significant correlation ($P > 0.05$). Gray scale reflects the magnitude of correlation, with gray denoting negative and black positive correlation. Data were taken from the TCGA database. n.s., nonsignificant.

(**Fig. 3A**). Furthermore, compared with miR-con, miR-149 mimics significantly downregulated CSF1 transcript levels in three different TNBC cell lines (**Fig. 3B**), translating into significantly reduced CSF1 protein amounts in the cell culture supernatant as measured by ELISA (**Fig. 3C**). These experiments confirm the direct regulation of the CSF1 mRNA by miR-149. The clinical relevance of this regulation is underscored by the inverse correlation of CSF1 and the macrophage markers CD163 and CD68 with miR-149 particularly in lymph node–positive compared with lymph node–negative TNBC tissues (**Fig. 3D** and **E**).

miR-149 suppresses CSF1-dependent communication between breast cancer cells and THP-1 macrophages

To address how miR-149 influences the communication between breast cancer cells and macrophages, we first analyzed in Transwell assays the chemotactic behavior of THP-1 MΦ triggered by CM derived from MDA-MB-231 cells transfected with either miR-con or miR-149 (**Fig. 4A**). In agreement with the suppression of CSF1 expression by miR-149, the chemotactic migration of THP-1 MΦ toward CM from MDA-MB-231 cells transfected with miR-149 mimics was significantly reduced compared with that of CM derived from the control cells. Notably, the reduction of chemotactic migration by miR-149 was comparable with the one observed upon siRNA-mediated knockdown of CSF1 (**Fig. 4B** and **C**). CM from BT-549 cells transfected with miR-149 was also less potent in stimulating the chemotaxis of THP MΦ when compared with the CM from control cells (Supplementary Fig. S2B and S2C).

To provide biochemical evidence for the reduced activation of THP-1 MΦ in response to CM from MDA-MB-231 cells transfected with miR-149, the CSF1R was immunoprecipitated from whole-cell lysates of THP-1 MΦ, followed by analysis of receptor tyrosine phosphorylation (**Fig. 4D**). The direct stimulation of THP-1 MΦ cells with CSF1 served as a positive control. Incubation of THP-1 MΦ with CM derived from MDA-MB-231 cells transfected with miR-con increased the phosphorylation of the CSF1R by approximately 5-fold compared with the control macrophages stimulated with non-conditioned medium. Importantly, stimulation of macrophages with CM derived from MDA-MB-231 cells transfected with miR-149 mimics or CSF1-specific siRNA induced a much weaker increase in CSF1R phosphorylation (**Fig. 4D**; 2.6- and 2.1-fold, respectively). These experiments demonstrate that the presence of

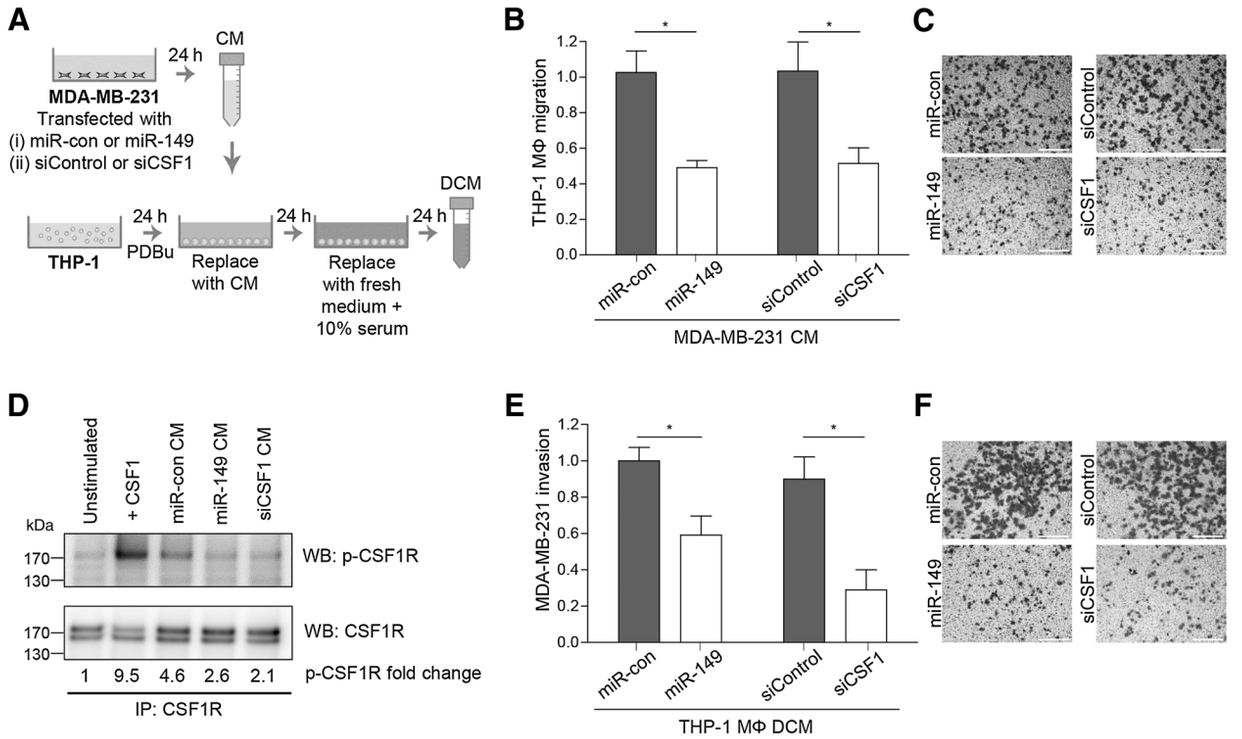

Figure 4.

miR-149 suppresses CSF1-dependent paracrine signaling between MDA-MB-231 cells and THP-1 cells. **A,** Scheme of the workflow. MDA-MB-231 cells were transiently transfected with miR-con or miR-149 mimics, a nontargeting siRNA control (siControl) or CSF1-specific siRNA (siCSF1). **B** and **D,** CM was used as a chemoattractant for THP-1 MΦ in a Transwell migration assay (**B**) or to stimulate THP-1 MΦ, followed by CSF1R immunoprecipitation from cell lysates and immunoblotting (**D**). The membrane was probed with a phosphotyrosine-specific antibody (pTyr99) and then reprobed with a CSF1R-specific antibody. Western blots of three independent experiments were quantified using ImageJ; the fold change (mean) in CSF1R phosphorylation was determined by normalizing the p-CSFR1/CSFR1 ratios to that of unstimulated samples. **E,** Double conditioned medium (DCM) was used as a chemoattractant for MDA-MB-231 cells in a Transwell invasion assay. Representative images of THP-1 MΦ migration (**C**) and MDA-MB-231 invasion assays (**F**). Scale bar, 200 μm. Data, mean ± SD, $n = 3$. *, $P \leq 0.05$; unpaired two-tailored Student t test.

miR-149 in MDA-MB-231 cells suppresses CSF1R activation in THP-1 MΦ by a paracrine mechanism.

To assess how the presence of miR-149 in MDA-MB-231 cells in turn affects the secretome of macrophages, we generated so-called double conditioned medium (DCM; **Fig. 4A**). Here, THP-1 MΦ were first stimulated with CM derived from MDA-MB-231 cells for 24 hours, before incubation of THP-1 MΦ with fresh medium for 24 hours (DCM). This medium was then used as a chemoattractant for parental MDA-MB-231 cells in invasion assays. Compared with the miRNA control condition, the invasion of parental MDA-MB-231 cells was strongly and significantly reduced by the initial transfection of MDA-MB-231 cells with miR-149 mimics. Again, the reduction observed was similar to the one upon CSF1 knockdown (**Fig. 4E** and **F**).

miR-149 suppresses EGFR ligand production by and M2 polarization of primary human macrophages

CSF1 stimulation of macrophages has been described to promote the secretion of EGFR ligands, which in turn stimulate EGFR-expressing cancer cells. To investigate this signaling loop, we set up a coculture assay in which breast cancer cells were seeded in the top and undifferentiated THP-1 cells in the bottom chamber of a Transwell, enabling the exchange of secreted factors while at the same time physically separating the cells. After 3 days of coculture, most of the THP-1 cells cocultured with MDA-MB-231 miR-con cells became adherent, although the number of adherent THP-1 cells was reduced when cocultured with MDA-MB-231 cells transfected with miR-149 mimics. In both cases, however, adherent THP-1 cells demonstrated increased cellular size, protrusions, and granularity, changes that reflect macrophage-like differentiation (24). After 3 days, we harvested the adherent THP-1 cells and analyzed the expression of the EGFR ligands EGF and amphiregulin (AREG) by quantitative RT-PCR. In THP-1 cells cocultured with MDA-MB-231 cells transfected with miR-149 mimics, the levels of EGF and AREG were strongly reduced compared with those measured in THP-1 cells cocultured with the MDA-MB-231 control cells (**Fig. 5A**). In parallel, we analyzed the EGFR phosphorylation levels (pY1086) in the cocultured MDA-MB-231 cells. In MDA-MB-231 cells transfected with miR-149, the EGFR phosphorylation level was much lower than the one observed in the MDA-MB-231 control cells in coculture (**Fig. 5B**). Importantly, the presence of miR-149 in MDA-MB-231 cells grown in monoculture did not affect EGFR or phospho-EGFR levels (**Fig. 5B**), suggesting that the reduction of EGFR phosphorylation in these cells can be ascribed to the reduced EGF and AREG production by the cocultured THP-1 cells.

We next sought to validate our results with primary human macrophages (hMΦ) derived from CD14-positive monocytes isolated from peripheral blood of healthy donors. In full agreement with the data obtained with THP-1 cells, the migration of hMΦ was also significantly reduced when CM was derived from MDA-MB-231 or BT-549 cells transfected with miR-149 mimics rather than control

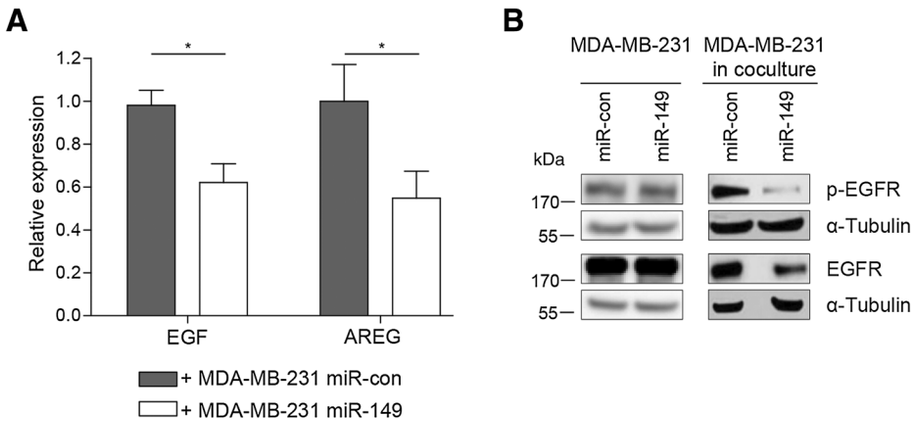

Figure 5.

miR-149 impairs paracrine signal cross-talk of MDA-MB-231 cells with THP-1 cells. MDA-MB-231 cells transiently transfected with miR-con or miR-149 mimics were seeded in the top chamber of a Transwell and cocultured with THP-1 monocytes contained in the bottom chamber. **A,** RNA was extracted from adherent THP-1 cells and EGF and AREG transcript levels were determined by qRT-PCR. Peptidylprolyl isomerase A and GAPDH were used as reference genes. Data, mean ± SD, $n = 3$. *, $P \leq 0.05$; unpaired two-tailored Student *t* test. **B,** After 3 days, MDA-MB-231 cells were lysed, and EGFR protein and phosphorylation (pY1086) were detected by immunoblotting. The membranes were reprobed with tubulin-specific antibody as a loading control.

miRNA (**Fig. 6A** and **B**; Supplementary Fig. S2D and S2E). Furthermore, compared with the basal expression levels in hMΦ, EGF and AREG were significantly upregulated after 1 day of coculture with MDA-MB-231 miR-con cells (**Fig. 6C**). Importantly, in the presence of MDA-MB-231 miR-149 cells, hMΦ failed to increase the expression of EGF and AREG (**Fig. 6C**). We next analyzed the expression of M1 and M2 macrophage markers to explore if the expression of miR-149 in MDA-MB-231 cells influences macrophage polarization. Compared with hMΦ in monoculture, the M2 marker genes mannose receptor C-type 1 (MRC1) and arginase-1 (ARG1) were strongly upregulated in hMΦ cocultured with MDA-MB-231 control cells (**Fig. 6D**). The expression of these genes was only modestly induced in hMΦ cocultured with MDA-MB-231 cells transfected with miR-149 mimics (**Fig. 6D**), whereas the M1 markers tumor necrosis factor alpha and indoleamine 2,3-dioxygenase were not significantly different between the groups (Supplementary Fig. S2F). Taken together, our data suggest that miR-149 expression in the breast cancer cells not only suppresses the CSF1/EGF cross-talk with primary human macrophages but also impairs M2 macrophage polarization.

miR-149 inhibits macrophage recruitment and lung metastasis of breast cancer cells *in vivo*

To investigate the suppression of macrophage recruitment by miR-149 *in vivo,* we generated MDA-MB-231 cells stably expressing a control miRNA and miR-149, respectively. In the stable MDA-MB-231 miR-149 cells, the levels of mature miR-149 were twice as high as the levels in the stable control cells, concomitant with strongly reduced CSF1 mRNA and protein levels (Supplementary Fig. S3A and S3B). In full agreement with our previous observations, CM derived from MDA-MB-231 miR-149 cells attracted fewer THP-1 MΦ than the CM from the stable MDA-MB-231 control cells, whereas the proliferation rates of the two stable cell lines were comparable (Supplementary

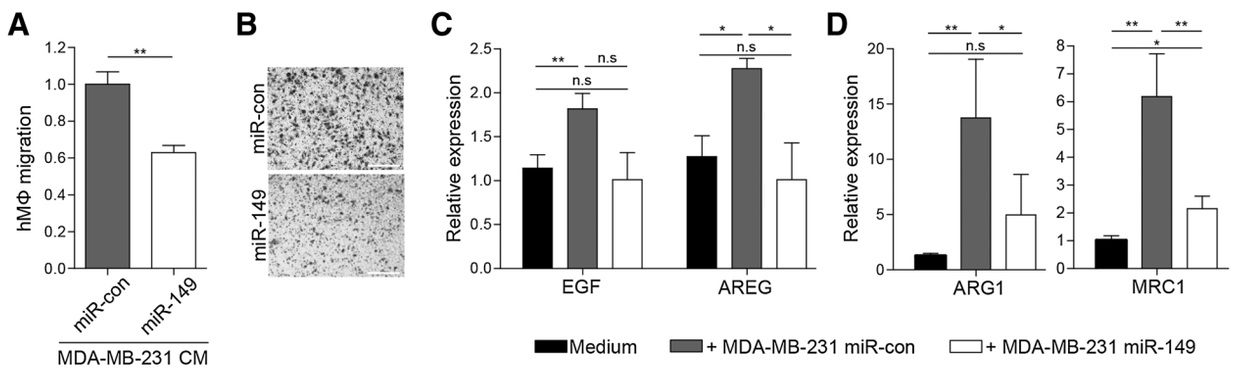

Figure 6.

miR-149 impairs breast cancer cell–induced migration of primary human macrophages, suppresses EGFR ligand expression, and induces M2 marker expression. **A,** CM of MDA-MB-231 cells transiently transfected with miR-con or miR-149 mimics was used as a chemoattractant for primary human macrophages (hMΦ) in a Transwell migration assay. **B,** Representative images of the Transwell migration assay. Scale bar, 200 μm. **C** and **D,** hMΦ were cocultured in a Transwell system with MDA-MB-231 cells transfected with miR-con or miR-149 mimics. After 24 hours, RNA from hMΦ was extracted and transcript levels of EGF and AREG (**C**) or MRC1 and ARG1 (**D**) were determined by qRT-PCR. Peptidylprolyl isomerase A and GAPDH were used as reference genes. Data, mean ± SD, $n = 3$. *, $P \leq 0.05$; **, $P \leq 0.01$; unpaired two-tailored Student *t* test (**A**) and one-way ANOVA (**C** and **D**). n.s., nonsignificant.

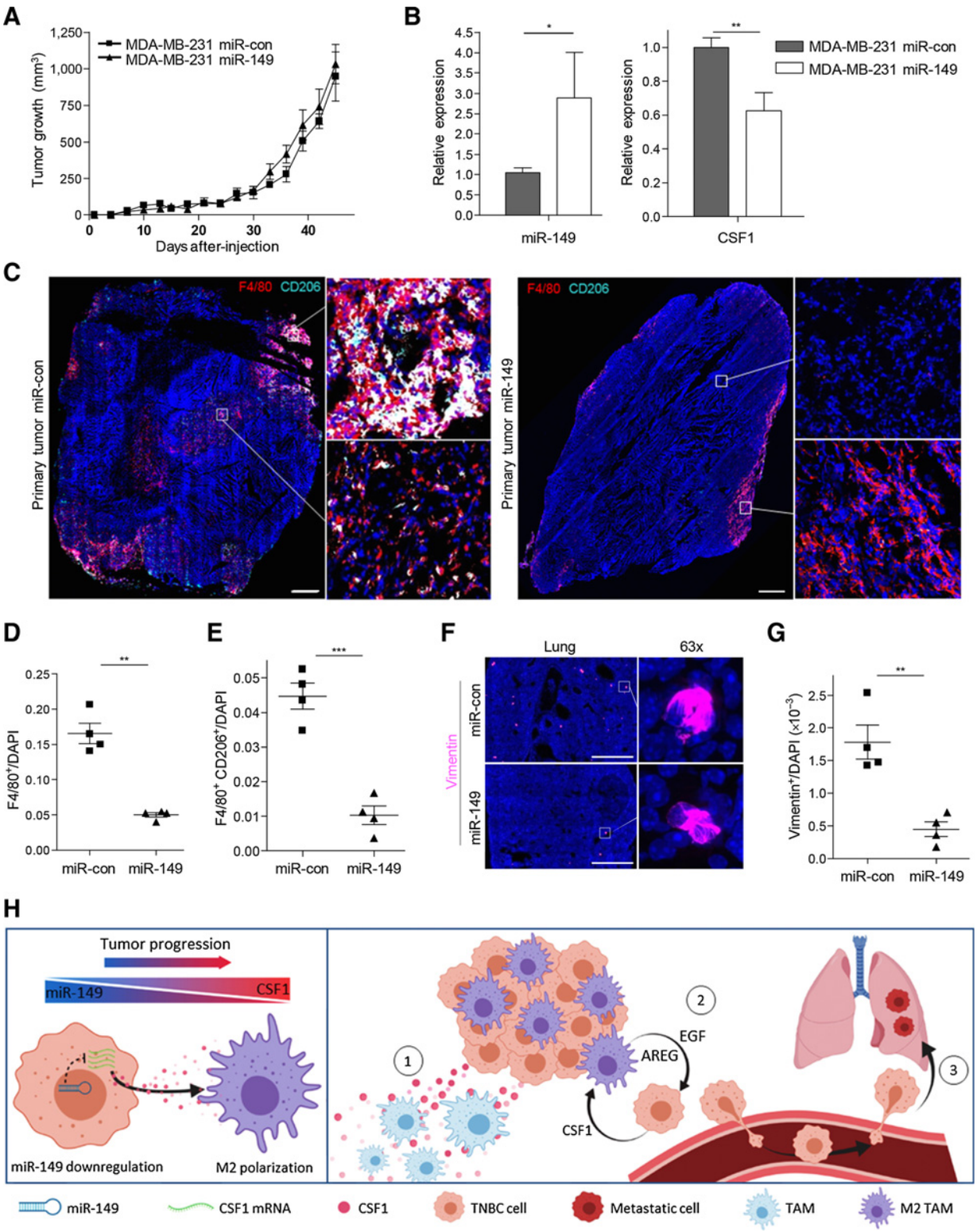

Fig. S3C and S3D). We then injected the stable MDA-MB-231 cell lines into the fourth mammary fat pad of SCID mice and monitored tumor growth over 6 weeks. All mice developed tumors, and no differences in tumor size were observed between the two groups (**Fig. 7A**). We then collected the tumors and measured the abundance of miR-149 and its target gene CSF1 in three individual tumors from each group. qRT-PCR analysis revealed that the suppression of CSF1 was maintained in the tumors formed by MDA-MB-231 miR-149 cells and inversely correlated with miR-149 expression (**Fig. 7B**).

To analyze the degree of macrophage infiltration, the primary tumors were transversally cryosectioned and stained by immunofluorescence for the general macrophage marker F4/80. To ensure that our analysis was not flawed by local differences in tumor heterogeneity, entire cryosections were imaged, resulting in approximately 600 images (20×) per cryosection, followed by software-based reconstruction of the cryosections and quantification of total F4/80 staining. In the control tumors, areas staining positively for F4/80 were frequently observed in both the periphery and central parts of the tumors. By contrast, only few F4/80-positive regions were detected in the tumors expressing miR-149, and these were restricted to the tumor periphery (**Fig. 7C** and **D**). To identify M2-polarized macrophages, we costained the tumor sections for F4/80 (red) and MRC1, corresponding to the CD206 antigen (turquoise). Quantification of F4/80 and CD206 double-positive areas revealed extensive infiltration of M2 macrophages in the miR-con tumors (red and turquoise), whereas hardly any M2 macrophages were detected in the tumors formed by MDA-MB-231 cells stably expressing miR-149 (**Fig. 7E**). Finally, to investigate whether miR-149 controlled metastasis development, lungs of tumor-bearing mice were longitudinally cryosectioned and stained with an anti-human vimentin antibody. Whole samples were imaged and analyzed as described for the primary tumors. Notably, vimentin staining of primary tumors expressing miR-149 was similar to that of control tumors, indicating that vimentin expression was not altered by miR-149 expression (Supplementary Fig. S3E). In comparison with the control, lung micrometastasis formation, as determined by vimentin staining, was significantly reduced in mice harboring primary tumors expressing miR-149 (**Fig. 7F** and **G**; Supplementary Fig. S3F). Taken together, our findings provide evidence that miR-149 functions as a metastasis-suppressing miRNA in breast cancer cells by limiting CSF1-dependent recruitment and M2 polarization of macrophages (**Fig. 7H**).

Discussion

Here, we identify miR-149 as a poor prognosis marker in TNBC that orchestrates the EGFR/CSF1R signaling axis between breast cancer cells and macrophages. In an orthotopic xenograft model of breast cancer we reveal a metastasis-suppressing function for miR-149 *in vivo*, which we believe is mediated in part by limiting CSF1-dependent recruitment of macrophages to the primary tumor. This conclusion is supported by clinical data analysis of primary breast cancers in which we find an inverse correlation between the expression of miR-149 and CSF1 as well as macrophage markers. In breast cancer, miR-149 downregulation has previously been reported to correlate with higher tumor stage (21, 22) and miR-149 was also found to be downregulated in lymph node metastases compared with paired primary tumors (22). We now show that low miR-149 expression significantly correlates with poor clinical outcomes in TNBC patients with lymph node-positive disease.

We and others have reported that miR-149 expression suppresses migration and invasion of breast cancer cells by regulating integrin signaling through the targeting of the Ras-related GTPases Rap1a/b and the Arf GTPase-activating protein GIT1 (21, 22). Our present study identifies another cancer hallmark to be regulated by miR-149, namely, tumor–stroma interactions involving macrophages. Infiltration of macrophages in cancer tissues is strongly associated with high vascular grade, poor prognosis and resistance to therapy (6, 36). CSF1 has been shown to play a key role in recruiting macrophages to the tumors and its overexpression in breast cancer patients correlates with poor prognosis (37). Here we present evidence that CSF1 is a *bona fide* target of miR-149. Our results show that low-level miR-149 reexpression in MDA-MB-231 cells suffices to suppress high CSF1 production by these cells, concomitant with the reduction of macrophage recruitment *in vitro* and *in vivo* (**Figs. 4** and **7**).

Apart from CSF1, additional chemokines such as C-C motif chemokine ligand 2 participate in monocyte and macrophage recruitment (7). Although siRNA-mediated downregulation of CSF1 mimicked the effects of miR-149 expression, we cannot rule out that additional factors involved in macrophage recruitment and/or differentiation contribute to the significantly reduced numbers of M2-like macrophages in the primary tumors expressing miR-149. In gastric cancer, for example, miR-149 has been reported to target interleukin (IL)-6 (38), and IL-6 is known to promote macrophage M2 activation by inducing IL-4 receptor expression (39). Considering that IL-6 is highly expressed in TNBC, the suppression of M2-macrophage polarization by miR-149 might result from the synergistic regulation of CSF1 and IL-6.

In response to CSF1 stimulation, TAMs have been shown to produce EGF, which augments the invasive properties and egress of breast cancer cells into blood vessels (12). Although the importance of this paracrine loop is widely accepted, the molecular mechanisms modulating this signaling cross-talk are poorly understood. Our data corroborate the importance of this paracrine pathway and show that miR-149 regulates the production of the EGFR ligands EGF and AREG

Figure 7.

Ectopic miR-149 expression in MDA-MB-231 cells inhibits macrophage recruitment and lung metastasis *in vivo*. MDA-MB-231 cells stably expressing a control miRNA or miR-149 were injected into the fourth mammary fat pad of SCID mice. **A,** Tumor growth was quantified every 3 days, and mice were sacrificed when the tumor reached 1.2 mm^3. **B,** RNA was extracted from tumor tissue, and miR-149 and CSF1 transcript levels were quantified by qRT-PCR. RNU6B and peptidylprolyl isomerase A were used as reference genes. **C,** Transversal cryosections of primary tumors were costained for F4/80 (red), CD206 (turquoise), and DAPI, followed by imaging using a spinning disk confocal microscope equipped with a Plan-Apochromat 20×/0.8. The images shown correspond to the assembly of approximately 600 individual images per cryosection. Scale bar, 1 mm. Zoom-in images show representative central and peripheral regions, respectively. **D** and **E,** $F4/80^+$ (**D**) and $F4/80^+$ $CD206^+$ (**E**) areas were quantified and normalized to the $DAPI^+$ areas (each value represents the analysis of three independent cryosections per tumor). **F,** Lung metastases were detected by staining for human vimentin, followed by imaging entire longitudinal lung cryosections using a spinning disk confocal microscope equipped with a Plan-Apochromat 10×/0.45 (scale bar, 0.5 mm). Images of representative micrometastases were acquired with a Plan-Apochromat 63×/1.40. **G,** $Vimentin^+$ areas were quantified and normalized to the $DAPI^+$ areas (each value represents the analysis of four independent cryosections per lung). **D, E,** and **G**, Data, mean ± SEM. $n = 4$ mice per group; *, $P \leq 0.05$; **, $P \leq 0.01$; ***, $P \leq 0.001$; unpaired two-tailored Student *t* test. **H,** Model describing that miR-149 downregulation in TNBC promotes tumor progression and metastasis by increasing CSF1-dependent recruitment and M2 polarization of TAMs, and by enhancing reciprocal EGF/CSF1 signaling between cancer cells and TAMs (created with BioRender.com).

by macrophages, ultimately determining EGFR activation levels in the breast cancer cells (**Figs. 5** and **6**). Interestingly, high AREG expression is associated with resistance to chemotherapeutic agents and breast cancer lymph node positivity (40, 41). A recent study described a podoplanin-positive M2-TAM subpopulation to be crucial for lymphangiogenesis. In breast cancer patients, association of these TAMs with tumor lymphatic vessels correlated with lymph node and distant metastasis (42). This might provide an explanation why low miR-149 levels and high macrophage infiltration correlate with poor prognosis, particularly in patients with lymph node–positive disease. Given that TAMs are essential for cancer cell dissemination through blood and lymph vessels (9, 42), it is likely that the reduced lung metastasis observed in our experiments upon miR-149 reexpression in MDA-MB-231 cells results from blocking metastasis via both hematogenous and lymphatic routes. M2-macrophage infiltration represents a negative prognosis factor in several advanced cancers, including gastric, thyroid, and glioblastoma (43, 44), where miR-149 has been reported to be downregulated. The regulation of tumor–macrophage interactions by miR-149 as uncovered by our study may thus not be limited to TNBC. In glioblastoma, for example, the CSF1/EGF paracrine loop with macrophages has been associated with microglia-induced glioblastoma invasion (45).

Metastasis development depends on cancer cell autonomous signaling and cancer cell interactions with the tumor microenvironment. Based on our data, we propose that miR-149 prevents metastatic dissemination of breast cancer cells by at least two mechanisms, i.e., controlling integrin signaling and cytoskeletal reorganization on the one hand (21, 22) and the communication with macrophages on the other hand, as shown in the present study. This is in accordance with the idea of miRNAs regulating a biological process by cotargeting multiple genes within interconnected signaling networks. For example, miR-148b was shown to control breast cancer progression and relapse by coordinating multiple genes involved in cell invasion and survival, including CSF1 (46). The tumor-suppressive function of miR-149 might additionally extend to the regulation of SEMA4D, although cancer cells do not appear to be the main source for this proangiogenic factor (47). Both single-nucleotide polymorphisms affecting miRNA maturation (48, 49) and DNA hypermethylation (38, 50) have been proposed as mechanisms contributing to miR-149 dysregulation in cancer. In future studies, it will be interesting to define by a global approach how miR-149 modulates gene expression and by which molecular mechanisms miR-149 is downregulated in TNBC.

Disclosure of Potential Conflicts of Interest

No potential conflicts of interest were disclosed.

Authors' Contributions

Conception and design: I. Sánchez-González, M. Strotbek, H. Busch, M.A. Olayioye
Development of methodology: I. Sánchez-González, A. Bobien, C. Molnar
Acquisition of data (provided animals, acquired and managed patients, provided facilities, etc.): I. Sánchez-González, A. Bobien, C. Molnar
Analysis and interpretation of data (e.g., statistical analysis, biostatistics, computational analysis): I. Sánchez-González, A. Bobien, C. Molnar, M. Strotbek, M. Boerries, H. Busch, M.A. Olayioye
Writing, review, and/or revision of the manuscript: I. Sánchez-González, M. Boerries, H. Busch, M.A. Olayioye
Administrative, technical, or material support (i.e., reporting or organizing data, constructing databases): I. Sánchez-González, S. Schmid, H. Busch
Study supervision: M.A. Olayioye

Acknowledgments

We thank Stephan Eisler (University of Stuttgart) for technical assistance with imaging and Angelika Hausser (University of Stuttgart) for discussions and critical reading of the manuscript. The lab of M.A. Olayioye is supported by grants by the Deutsche Forschungsgemeinschaft (DFG) and Deutsche Krebshilfe. M. Boerries is supported by the DFG (SFB 850) and the German Federal Ministry of Education and within the framework of the e:Med research and funding concept CoNfirm (FKZ 01ZX1708F to M. Boerries) and by MIRACUM within the Medical Informatics Funding Scheme (FKZ 01ZZ1801B to M. Boerries). H. Busch is funded by the DFG under Germany's Excellence Strategy, EXC 22167-390884018. I. Sánchez-González received a Conacyt-DAAD fellowship.

The costs of publication of this article were defrayed in part by the payment of page charges. This article must therefore be hereby marked *advertisement* in accordance with 18 U.S.C. Section 1734 solely to indicate this fact.

Received June 26, 2019; revised October 14, 2019; accepted January 2, 2020; published first January 7, 2020.

References

1. Nguyen DX, Bos PD, Massagué J. Metastasis: from dissemination to organ-specific colonization. Nat Rev Cancer 2009;9:274–84.
2. Hurvitz SA, Finn RS. What's positive about "triple-negative" breast cancer? Futur Oncol 2009;5:1015–25.
3. Di Cosimo S, Baselga J. Management of breast cancer with targeted agents: importance of heterogenicity. Nat Rev Clin Oncol 2010;7:139–47.
4. De Palma M, Biziato D, Petrova TV. Microenvironmental regulation of tumour angiogenesis. Nat Rev Cancer 2017;17:457–74.
5. Mantovani A, Sica A. Macrophages, innate immunity and cancer: balance, tolerance, and diversity. Curr Opin Immunol 2010:231–7.
6. Obeid E, Nanda R, Fu YX, Olopade OI. The role of tumor-associated macrophages in breast cancer progression. Int J Oncol 2013;43:5–12.
7. Mantovani A, Marchesi F, Malesci A, Laghi L, Allavena P. Tumour-associated macrophages as treatment targets in oncology. Nat Rev Clin Oncol 2017;14:399–416.
8. Laoui D, van Overmeire E, de Baetselier P, van Ginderachter JA, Raes G. Functional relationship between tumor-associated macrophages and macrophage colony-stimulating factor as contributors to cancer progression. Front Immunol 2014;5:1–15.
9. Condeelis J, Pollard JW. Macrophages: obligate partners for tumor cell migration, invasion, and metastasis. Cell 2006;124:263–6.
10. Harney AS, Arwert EN, Entenberg D, Wang Y, Guo P, Qian BZ, et al. Real-time imaging reveals local, transient vascular permeability, and tumor cell intravasation stimulated by TIE2hi macrophage–derived VEGFA. Cancer Discov 2015;5:932–43.
11. Lin BEY, Nguyen AV, Russell RG, Pollard JW. Colony-stimulating factor 1 promotes progression of mammary tumors to malignancy. J Exp Med 2001;193:727–40.
12. Goswami S, Sahai E, Wyckoff JB, Cammer M, Cox D, Pixley FJ, et al. Macrophages promote the invasion of breast carcinoma cells via a colony-stimulating factor-1/epidermal growth factor paracrine loop. Cancer Res 2005;65:5278–84.
13. DeNardo DG, Brennan DJ, Rexhepaj E, Ruffell B, Shiao SL, Madden SF, et al. Leukocyte complexity predicts breast cancer survival and functionally regulates response to chemotherapy. Cancer Discov 2011;1:54–67.
14. Kluger HM, Dolled-Filhart M, Rodov S, Barry M, Kacinski BM, Camp RL, et al. Macrophage colony-stimulating factor-1 receptor expression is associated with poor outcome in breast cancer by large cohort tissue microarray analysis. Clin Cancer Res 2004;10:173–7.
15. Shabo I, Stål O, Olsson H, Doré S, Svanvik J. Breast cancer expression of CD163, a macrophage scavenger receptor, is related to early distant recurrence and reduced patient survival. Int J Cancer 2008;123:780–6.
16. Bartel DP. MicroRNAs: target recognition and regulatory functions. Cell 2009;136:215–33.
17. Ambros V. The functions of animal microRNAs. Nature 2004;431:350–5.
18. Farazi TA, Hoell JI, Morozov P, Tuschl T. MicroRNAs in human cancer. Adv Exp Med Biol 2013;774:1–20.

19. Rupaimoole R, Slack FJ. MicroRNA therapeutics: towards a new era for the management of cancer and other diseases. Nat Rev Drug Discov 2017;16:203–21.
20. He Y, Yu D, Zhu L, Zhong S, Zhao J, Tang J. miR-149 in human cancer: a systemic review. J Cancer 2018;9:375–88.
21. Bischoff A, Huck B, Keller B, Strotbek M, Schmid S, Boerries M, et al. MiR149 functions as a tumor suppressor by controlling breast epithelial cell migration and invasion. Cancer Res 2014;74:5256–65.
22. Chan SH, Huang WC, Chang JW, Chang KJ, Kuo WH, Wang MY, et al. MicroRNA-149 targets GIT1 to suppress integrin signaling and breast cancer metastasis. Oncogene 2014;33:4496–507.
23. Linder S, Nelson D, Weiss M, Aepfelbacher M. Wiskott-Aldrich syndrome protein regulates podosomes in primary human macrophages. Proc Natl Acad Sci U S A 2002;96:9648–53.
24. Stewart DA, Yang Y, Makowski L, Troester MA. Basal-like breast cancer cells induce phenotypic and genomic changes in macrophages. Mol Cancer Res 2012; 10:727–38.
25. Dyer BW, Ferrer FA, Klinedinst DK, Rodriguez R. A noncommercial dual luciferase enzyme assay system for reporter gene analysis. Anal Biochem 2000; 282:158–61.
26. Rahman M, Jackson LK, Johnson WE, Li DY, Bild AH, Piccolo SR. Alternative preprocessing of RNA-Sequencing data in the Cancer Genome Atlas leads to improved analysis results. Bioinformatics 2015;31:3666–72.
27. Anaya J. OncoLnc: linking TCGA survival data to mRNAs, miRNAs, and lncRNAs. PeerJ Comput Sci 2016;2:e67.
28. Dweep H, Gretz N. miRWalk2.0: a comprehensive atlas of microRNA-target interactions. Nat Methods 2015;12:697.
29. Ashburner M, Ball CA, Blake JA, Botstein D, Butler H, Cherry JM, et al. Gene ontology: tool for the unification of biology. The Gene Ontology Consortium. Nat Genet 2000;25:25–9.
30. Blake JA, Christie KR, Dolan ME, Drabkin HJ, Hill DP, Ni L, et al. Gene ontology consortium: going forward. Nucleic Acids Res 2015;43:D1049–56.
31. Ben-Hamo R, Efroni S. MicroRNA regulation of molecular pathways as a generic mechanism and as a core disease phenotype. Oncotarget 2015;6:1594–604.
32. Basile JR, Barac A, Zhu T, Guan KL, Gutkind JS. Class IV semaphorins promote angiogenesis by stimulating Rho-initiated pathways through plexin-B. Cancer Res 2004;64:5212–24.
33. Aran D, Hu Z, Butte AJ. xCell: digitally portraying the tissue cellular heterogeneity landscape. Genome Biol 2017;18:220.
34. Auwerx J. The human leukemia cell line, THP-1: a multifacetted model for the study of monocyte-macrophage differentiation. Experientia 1991;47:22–31.
35. Daigneault M, Preston JA, Marriott HM, Whyte MKB, Dockrell DH. The identification of markers of macrophage differentiation in PMA-stimulated THP-1 cells and monocyte-derived macrophages. PLoS One 2010;5:e8668.
36. Quigley DA, Kristensen V. Predicting prognosis and therapeutic response from interactions between lymphocytes and tumor cells. Mol Oncol 2015;9:2054–62.
37. Lin EY, Gouon-Evans V, Nguyen AV, Pollard JW. The macrophage growth factor CSF-1 in mammary gland development and tumor progression. J Mammary Gland Biol Neoplasia 2002;7:147–62.
38. Li P, Shan JX, Chen XH, Zhang D, Su LP, Huang XY, et al. Epigenetic silencing of microRNA-149 in cancer-associated fibroblasts mediates prostaglandin E2/interleukin-6 signaling in the tumor microenvironment. Cell Res 2015;25: 588–603.
39. Mauer J, Chaurasia B, Goldau J, Vogt MC, Ruud J, Nguyen KD, et al. Interleukin-6 signaling promotes alternative macrophage activation to limit obesity-associated insulin resistance and endotoxemia. Nat Immunol 2012;29:997–1003.
40. Berasain C, Avila MA. Amphiregulin. Semin Cell Dev Biol 2014;28:31–41.
41. Eckstein N, Servan K, Girard L, Cai D, Von Jonquieres G, Jaehde U, et al. Epidermal growth factor receptor pathway analysis identifies amphiregulin as a key factor for cisplatin resistance of human breast cancer cells. J Biol Chem 2008; 283:739–50.
42. Bieniasz-Krzywiec P, Martín-Pérez R, Ehling M, García-Caballero M, Pinioti S, Pretto S, et al. Podoplanin-expressing macrophages promote lymphangiogenesis and lymphoinvasion in breast cancer. Cell Metab 2019;30:1–20.
43. Zhang QW, Liu L, Gong CY, Shi HS, Zeng YH, Wang XZ, et al. Prognostic significance of tumor-associated macrophages in solid tumor: a meta-analysis of the literature. PLoS One 2012;7:e50946.
44. Hambardzumyan D, Gutmann DH, Kettenmann H. The role of microglia and macrophages in glioma maintenance and progression. Nat Neurosci 2015;19:20–7.
45. Coniglio SJ, Eugenin E, Dobrenis K, Stanley ER, West BL, Symons MH, et al. Microglial stimulation of glioblastoma invasion involves epidermal growth factor receptor (EGFR) and colony stimulating factor 1 receptor (CSF-1R) signaling. Mol Med 2012;18:519–27.
46. Cimino D, De Pittà C, Orso F, Zampini M, Casara S, Penna E, et al. miR148b is a major coordinator of breast cancer progression in a relapse-associated microRNA signature by targeting ITGA5, ROCK1, PIK3CA, NRAS, and CSF1. FASEB J 2013;27:1223–35.
47. Sierra JR, Corso S, Caione L, Cepero V, Conrotto P, Cignetti A, et al. Tumor angiogenesis and progression are enhanced by Sema4D produced by tumor-associated macrophages. J Exp Med 2008;205:1673–85.
48. Tu HF, Liu CJ, Chang CL, Wang PW, Kao SY, Yang CC, et al. The association between genetic polymorphism and the processing efficiency of miR-149 affects the prognosis of patients with head and neck squamous cell carcinoma. PLoS One 2012;7:e51606.
49. Li L, Sheng Y, Lv L, Gao J. The association between two MicroRNA variants (miR-499, miR-149) and gastrointestinal cancer risk: a meta-analysis. PLoS One 2013;8:1–10.
50. Wang F, Ma YL, Zhang P, Shen TY, Shi CZ, Yang YZ, et al. SP1 mediates the link between methylation of the tumour suppressor miR-149 and outcome in colorectal cancer. J Pathol 2013;229:12–24.